

Article

Fabrication of (Ge_{0.42}Sn_{0.58})S Thin Films via Co-Evaporation and Their Solar Cell Applications

Daiki Motai and Hideaki Araki *

National Institute of Technology (KOSEN), Nagaoka College, Niigata 940-8532, Japan

* Correspondence: h-araki@nagaoka-ct.ac.jp

Abstract: In this study, as a novel approach to thin-film solar cells based on tin sulfide, an environmentally friendly material, we attempted to fabricate (Ge, Sn)S thin films for application in multi-junction solar cells. A (Ge_{0.42}Sn_{0.58})S thin film was prepared via co-evaporation. The (Ge_{0.42}Sn_{0.58})S thin film formed a (Ge, Sn)S solid solution, as confirmed by X-ray diffraction (XRD) and Raman spectroscopy analyses. The open circuit voltage (V_{oc}), short circuit current density (J_{sc}), fill factor (FF), and power conversion efficiency (PCE) of (Ge_{0.42}Sn_{0.58})S thin-film solar cells were 0.29 V, 6.92 mA/cm², 0.34, and 0.67%, respectively; moreover, the device showed a band gap of 1.42–1.52 eV. We showed that solar cells can be realized even in a composition range with a relatively higher Ge concentration than the (Ge, Sn)S solar cells reported to date. This result enhances the feasibility of multi-junction SnS-system thin-film solar cells.

Keywords: SnS; (Ge, Sn)S; solid solution; co-evaporation method

1. Introduction

Developing energy resources to replace fossil fuels is an important goal of current energy research. Photovoltaic (PV) power generation is a promising technology for sustainable energy production. As the demand for renewable energy increases, there is a need to increase the number of solar cell installations and to fabricate higher efficiency solar cells. To increase the number of solar cell installations, solar cells need to be light and flexible enough to be installed in previously impossible places, such as on curved surfaces or delicate buildings. This can be achieved by making the material thinner and forming it on a flexible substrate; therefore, compound thin-film semiconductors that can sufficiently absorb light are attracting research attention. Multi-junction compound solar cells consisting of materials with different band gaps have been widely studied and demonstrated to absorb sunlight efficiently. The light-absorbing layers of such multi-junction solar cells should exhibit adjustable bandgaps. Thin-film solar cells fabricated with one such material, Cu(In,Ga)Se₂ (CIGS), exhibited a power conversion efficiency of over 23% [1]. However, CIGS contains several rare metals, such as the toxic elements Se, In, and Ga, and the resource constraints and environmental impact of its mass production are concerning. It is therefore vital to develop new alternative materials. Thus, this study focuses on a compound semiconductor—a tin sulfide (SnS)-based compound—which can be an alternative to CIGS regarding resources, cost, and environment.

SnS is a binary chalcogenide compound composed of tin and sulfur. It shows high potential as an environmentally friendly material because it is composed of low-toxicity elements abundant in the Earth's crust. The structural polymorphism of SnS at room temperature is known to be orthorhombic SnS (Pnma), rock salt SnS (P213), and sphalerite SnS (F-43 m) [2–5]. This study focuses on the most studied form, orthorhombic SnS. Note that from here on, orthorhombic SnS is denoted as SnS.

SnS thin films can be prepared by various methods, including thermal evaporation [6,7], co-evaporation [8–10], sputtering [11–14], sulfurization [15,16], atomic layer



Citation: Motai, D.; Araki, H.

Fabrication of (Ge_{0.42}Sn_{0.58})S Thin Films via Co-Evaporation and Their Solar Cell Applications. *Materials* **2024**, *17*, 692. <https://doi.org/10.3390/ma17030692>

Academic Editor: Sheikh A. Akbar

Received: 30 July 2023

Revised: 28 January 2024

Accepted: 29 January 2024

Published: 1 February 2024



Copyright: © 2024 by the authors. Licensee MDPI, Basel, Switzerland. This article is an open access article distributed under the terms and conditions of the Creative Commons Attribution (CC BY) license (<https://creativecommons.org/licenses/by/4.0/>).

deposition [17–19], and chemical bath deposition [20]. This indicates that SnS has a high degree of freedom in fabrication methods. In addition, SnS exhibits a band gap of 1.3 eV [8,9,15,21–23] and a high absorption coefficient [21,23]. This means that SnS is suitable for use in the light-absorbing layers of solar cells.

The development history of solar cells using SnS is described briefly below. In 1994, Noguchi et al., produced the first solar cell (ITO/n-CdS/p-SnS/Ag structure) using a SnS film and reported that it exhibited photovoltaic properties [21]. In 2006, Reddy fabricated a SnS thin-film solar cell with a SnO₂/p-SnS/CdS/ITO structure and showed a PCE of 1.3% [24]. In 2013, Ikuno et al. fabricated a super straight type SnS thin-film solar cell with an ITO/Zn_{1-x}Mg_xO/p-SnS/Cu structure and reported a conversion efficiency of 2.1% [25]. A year later, Sinsersuksakul et al., fabricated a substrate-type Mo/p-SnS/SnO₂/Zn(O,S):N/ZnO/ITO structure cell that showed a conversion efficiency of 4.36% [18], significantly improving the performance of SnS thin-film solar cells. Despite the steady improvement in conversion efficiency, it has stagnated in the 4% range [26,27], and research on solar cell applications of SnS is at a low ebb. However, novel approaches have been recently investigated for developing SnS solar cell applications. Here, we present two state-of-the-art approaches for SnS solar cells.

The first is the preparation of SnS with n-type conduction and its application to homojunction solar cells. SnS usually exhibits p-type conduction because tin vacancies (V_{Sn}) in the sulfur-rich state and tin sulfur antisite (Sn_S) in the tin-rich state behave as acceptor-type defects [13,28]. Yanagi et al. succeeded in preparing bulk SnS with n-type conduction by doping Cl [29], and Suzuki et al. reported that n-type SnS thin films can be prepared by supplying sulfur plasma while sputtering Cl-doped SnS [13]. Furthermore, Kawanishi et al. have achieved the fabrication of homojunction solar cells by employing p-type SnS thin films and n-type SnS single crystals [14].

The second is the preparation of SnS with a bandgap tunable for application to multi-junction solar cells. Regarding fabricating high-efficiency solar cells, multi-junction compound solar cells consisting of materials with different band gaps have been widely studied and were demonstrated to absorb sunlight efficiently. The light-absorbing layers of such multi-junction solar cells should exhibit adjustable bandgaps. Very recently, Kawamura et al. have succeeded in broadening the bandgap of SnS to ~2.25 eV by solid-dissolving alkaline earth metals in SnS [30].

Thus, SnS solar cells have again attracted attention in recent years due to novel approaches that take advantage of their potential capabilities.

In this study, as an approach to wide-bandgap SnS, we attempted to fabricate a (Ge, Sn)S thin-film solar cell by dissolving Ge in SnS. (Ge, Sn)S, a solid solution of SnS and germanium sulfide (GeS), shows a tunable band gap (between 1.3 and 1.6 eV) in its nanocrystals depending on the Ge concentration [31]. However, there have been very few reports on fabricating (Ge, Sn)S thin films; therefore, this topic requires further investigation. A previous study reported the fabrication of (Ge_x Sn_{1-x})S ($x = 0.18, 0.27$) thin films via co-evaporation and their application in thin-film solar cells [32]. Our study reports the fabrication and solar cell applications of (Ge_x Sn_{1-x})S thin films containing more Ge than previously reported. We then discuss the Ge solid solution effect by comparing it with the SnS we fabricated in the past [32].

2. Materials and Methods

Molybdenum disks (Mo, 99.95%, 3-mm thick, Furuuchi Chemical Corporation, Tokyo, Japan), tin shots (99.9999%, Furuuchi Chemical Corporation, Tokyo, Japan), germanium shots (99.999%, Furuuchi Chemical Corporation, Tokyo, Japan), sulfur chunks (S, 99.9999%, Furuuchi Chemical Corporation, Tokyo, Japan), cadmium iodide (CdI₂, 99%, FUJIFILM Wako Pure Chemical Corporation, Osaka, Japan), thiourea (CS(NH₂)₂, 98%, Nacalai Tesque Inc., Kyoto, Japan), ammonia water (NH₃, 28 wt%, FUJIFILM Wako Pure Chemical Corporation, Osaka, Japan), ZnO: Al (Al₂O₃ = 2 wt%, 3-mm thick, 99.99%, Furuuchi Chemical

Corporation, Tokyo, Japan), and aluminum (Al, 99.99%, The Nilaco Corporation, Tokyo, Japan) were used as purchased.

First, approximately 0.8 μm Mo was deposited as the bottom electrode on an ultrasonically cleaned Eagle XG (Corning, Corning, NY, USA) substrate using DC sputtering (deposition time; 25 min, applied current; 1.0 A, process pressure; 0.4 Pa, Ar flow; 20 sccm). The deposition was performed under the same sputtering conditions under which the Mo thin film with a resistivity of 3.6×10^{-5} ohm/cm was obtained. Subsequently, SnS and $(\text{Ge}_x\text{Sn}_{1-x})\text{S}$ thin films were deposited by the co-evaporation of Ge, Sn, and S at pressures on the order of 10^{-4} Pa for 3 h using independent deposition sources. Sulfur is typically supplied as S_8 molecules; however, to ensure a higher supply of reactive sulfur, S_8 molecules were decomposed into S_x by thermal cracking at 800 °C. Table 1 lists the manufacturing conditions in detail.

Table 1. Film fabrication conditions for the co-evaporation process.

| | SnS [32] | $(\text{Ge}_x\text{Sn}_{1-x})\text{S}$ |
|----------------------------|----------|--|
| Deposition time [hours] | 3 | 3 |
| Ge cell temperature [°C] | - | 1200 |
| Sn cell temperature [°C] | 1015 | 1010 |
| S temperature [°C] | 150 | 150 |
| Substrate temperature [°C] | 300 | 150 |
| S-Valve opening | 3 | 1.5 |

$(\text{Ge}_x\text{Sn}_{1-x})\text{S}$ thin films were fabricated under lower substrate temperature conditions (150 °C) than those used to synthesize SnS thin films to suppress the re-evaporation of GeS (which exhibits a high vapor pressure).

The as-prepared $(\text{Ge}_x\text{Sn}_{1-x})\text{S}$ thin films were annealed under a nitrogen atmosphere (the process pressure was atmospheric pressure, 1×10^5 Pa) in an infrared heating furnace. The temperature profile during annealing is shown in Figure 1. The fabricated thin films were analyzed using X-ray fluorescence spectroscopy (XRF, ZSX Primus IV, Rigaku Corporation, Tokyo, Japan), X-ray diffraction (XRD, MiniFlex, Rigaku Corporation, Tokyo, Japan), and Raman spectroscopy (RMP-510, JASCO Corporation, Tokyo, Japan) at an excitation wavelength of 532 nm, and scanning electron microscopy (SEM, JSM-6060LV, JEOL Ltd., Tokyo, Japan).

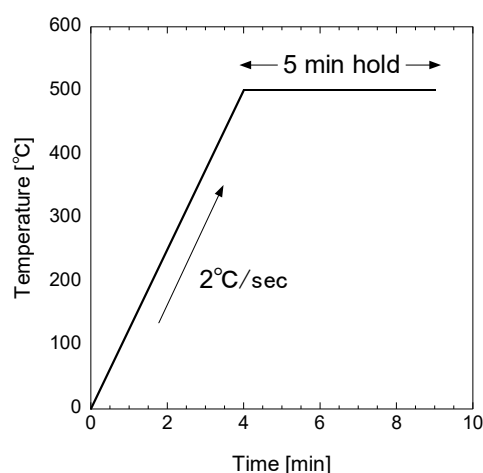


Figure 1. Temperature profile during the annealing of $(\text{Ge}_x\text{Sn}_{1-x})\text{S}$ thin films.

Subsequently, an n-type CdS buffer layer approximately 90 nm thick was deposited on the $(\text{Ge}_x\text{Sn}_{1-x})\text{S}$ absorption layer by the CBD method at 70 °C for 20 min using a solution consisting of cadmium iodide (CdI_2 ; 3.58 mmol L^{-1}), ammonia water (NH_3 ; 2.83 mol L^{-1}), and thiourea ($(\text{NH}_2)_2\text{CS}$; 0.298 mol L^{-1}). The fabricated $(\text{Ge}_x\text{Sn}_{1-x})\text{S}$ /CdS thin films

were annealed in air at 200 °C for 20 min [33]. Next, Al-doped zinc oxide (ZnO:Al) was deposited as a window layer by radio frequency sputtering (deposition time; 110 min, RF power; 100 W, process pressure; 0.5 Pa, Ar flow; 20 sccm). The deposition was performed under the same sputtering conditions under which the ZnO:Al thin film was obtained with a thickness of approximately 450 nm, a resistivity of 1×10^{-4} ohm/cm, and a transmittance of >80% in the visible light wavelength range 400–1000 nm. Finally, Al was deposited as the top electrode by thermal evaporation.

The final thin-film solar cells with an Eagle XG/Mo/SnS or $(\text{Ge}_x \text{Sn}_{1-x})\text{S}/\text{CdS}/\text{ZnO:Al}/\text{Al}$ structure were scribed into cells with an approximate size of 4.4 mm \times 4.4 mm (aperture area ~ 0.16 cm²). The photovoltaic characteristics of the fabricated solar cells were evaluated using a solar simulator (SX-UI 500XQ, Ushio Inc., Tokyo, Japan) under AM 1.5 and 100 mW/cm² irradiation. The external quantum efficiency (EQE) of the fabricated solar cells was evaluated using a solar cell evaluation system (SML-250 J, Bunkoukeiki Co., Ltd., Tokyo, Japan).

3. Results and Discussion

The elemental compositions of the fabricated SnS and $(\text{Ge}_x \text{Sn}_{1-x})\text{S}$ thin films were analyzed by XRF, as summarized in Table 2. The average composition in a ϕ 20-mm diameter plane near the center of a 25 mm \times 25 mm sample was evaluated, and a summary of the compositional ratios is given. The composition of the thin films was estimated using analysis software (ZSX Primus IV, Rigaku Co., Tokyo, Japan) based on the fundamental parameter method. The error in the composition values of Sn, Ge, and S is less than 1% in repeated measurements of the same sample. The SnS film was thinner than the $(\text{Ge}_x \text{Sn}_{1-x})\text{S}$ film, possibly due to the re-evaporation of SnS during fabrication, which was carried out at a substrate temperature of 300 °C. The Ge/(Ge + Sn) composition ratio of the $(\text{Ge}_x \text{Sn}_{1-x})\text{S}$ thin film was estimated to be 0.42; the thin film has been subsequently denoted as $(\text{Ge}_{0.42} \text{Sn}_{0.58})\text{S}$. For the $(\text{Ge}_{0.42} \text{Sn}_{0.58})\text{S}$ thin film, annealing decreased the film thickness and increased the (Ge + Sn)/S composition ratio, although its Ge/(Ge + Sn) composition ratio remained unchanged. This could be attributed to the re-evaporation of sulfur during annealing. The S-rich composition compared to stoichiometric composition was confirmed for both SnS and $(\text{Ge}_{0.42} \text{Sn}_{0.58})\text{S}$. According to a previously published first-principles study, S-rich SnS is more likely to form tin vacancy (V_{Sn}) defects at shallow energy levels than sulfur vacancy (V_{S}) and sulfur antisite tin (Sn_{S}) defects at deep energy levels [34]. Therefore, it is speculated that the fabricated SnS thin film had relatively fewer V_{S} , which can serve as recombination centers, and a thin film with excellent potential was fabricated.

Table 2. Film thicknesses and constituent-element compositions estimated by XRF.

| | Thickness [μm] | Ge/(Ge + Sn) | (Ge + Sn)/S |
|--|-----------------------------|--------------|-------------|
| SnS [32] | 0.687 | 0 | 0.98 |
| $(\text{Ge}_x \text{Sn}_{1-x})\text{S}$ (As deposited) | 1.087 | 0.42 | 0.95 |
| $(\text{Ge}_x \text{Sn}_{1-x})\text{S}$ (Annealed) | 1.033 | 0.42 | 0.98 |

Figure 2a shows the XRD patterns of the fabricated SnS and $(\text{Ge}, \text{Sn})\text{S}$ thin films. XRD measurements were performed using MiniFlex with a NaI scintillation counter used as a detector. This apparatus has a vertical goniometer with a radius of 150 mm and an accuracy of $\pm 0.02^\circ$. The measurement parameters were as follows: X-ray = 30 kV/15 mA, divergence slit (DS) = variable, scattering slit (SS) = 4.2° , receiving slit (RS) = 0.3 mm, and K_{β} foil filter. The measurement range was 10–90° with a step of 0.01° . The pattern of the fabricated SnS thin film was similar to that of orthorhombic SnS, while the $(\text{Ge}_{0.42} \text{Sn}_{0.58})\text{S}$ thin film exhibited peaks at 31.27° , 32.37° , and 32.90° , as shown in Figure 2b. These peaks could be attributed to the (101), (111), and (040) planes of a $(\text{Ge}, \text{Sn})\text{S}$ solid solution, or to the different phases of Sn_2S_3 , GeS, and GeS_2 . A plot of the estimated lattice constant of the b -axis for the most intense peak at 32.90° is shown in Figure 2c. The estimated lattice constant b , calculated using the ICDD Powder Diffraction File for SnS and GeS (PDF SnS #00-039-0354

and GeS #00-051-1168), roughly followed the Vegard rule; thus, a (Ge, Sn)S solid solution was formed in the $(\text{Ge}_{0.42}\text{Sn}_{0.58})\text{S}$ thin film. Moreover, as shown in Figure 2a, a peak at 12.90° (possibly due to Sn_2S_3) was observed in the XRD spectrum of the $(\text{Ge}_{0.42}\text{Sn}_{0.58})\text{S}$ thin film; here, the peak appeared at a higher angle than its position in the reference (Sn_2S_3 #00-014-0619) spectrum, probably because a part of Sn_2S_3 was substituted by Ge to form $(\text{Ge, Sn})_2\text{S}_3$.

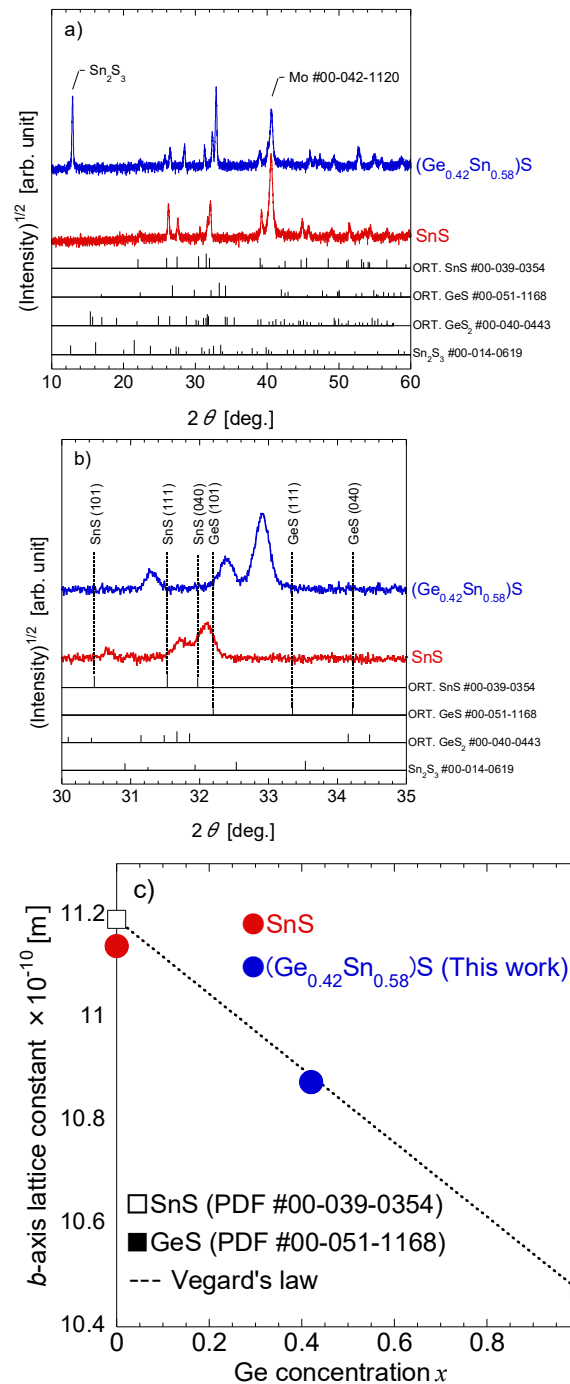


Figure 2. (a) XRD patterns of the fabricated SnS [32] and $(\text{Ge}_{0.42}\text{Sn}_{0.58})\text{S}$ thin films. The relevant PDF cards are shown at the bottom of the figure as a reference. (b) Magnified views of the XRD patterns are shown in the range of $30\text{--}35^\circ$ (Red line: SnS thin film, blue line: $(\text{Ge}_{0.42}\text{Sn}_{0.58})\text{S}$ thin film). (c) Dependence of the b -axis lattice constant on Ge concentration. The lattice constant b is calculated from the peak assigned to the (040) plane.

Figure 3 shows the Raman spectra of the SnS [32] and $(\text{Ge}_{0.42}\text{Sn}_{0.58})\text{S}$ thin films. The spectral peaks of the SnS thin film could be attributed to orthorhombic SnS; peaks were observed at 95.9 cm^{-1} (A_g), 164.0 cm^{-1} (B_{3g}), 192.0 cm^{-1} (A_g), and 219.5 cm^{-1} (A_g) (the vibrational modes are indicated in brackets) [35]. No peaks attributable to GeS and SnS_2 were observed [36,37]. A higher-wavenumber peak shift was observed in the $(\text{Ge}_{0.42}\text{Sn}_{0.58})\text{S}$ spectrum; this could be attributed to the substitution of the Sn sites in SnS by Ge. A similar shift of Raman peaks has been reported by Araki et al. in a similar sulfide solid solution, $\text{Cu}_2(\text{Ge}_x\text{Sn}_{1-x})\text{S}_3$, which is attributed to the substitution of Sn by Ge [38]. Therefore, a (Ge, Sn)S solid solution was formed in the $\text{Ge}_x\text{Sn}_{1-x}\text{S}$ system in this study, even with a Ge composition corresponding to a high Ge/(Ge + Sn) ratio of 0.42. Raman spectroscopy did not indicate any of the different phases (such as GeS_2 or Sn_2S_3) indicated by XRD analysis; thus, it is suggested that (Ge, Sn)S predominantly existed near the surface of the $(\text{Ge}_{0.42}\text{Sn}_{0.58})\text{S}$ thin film.

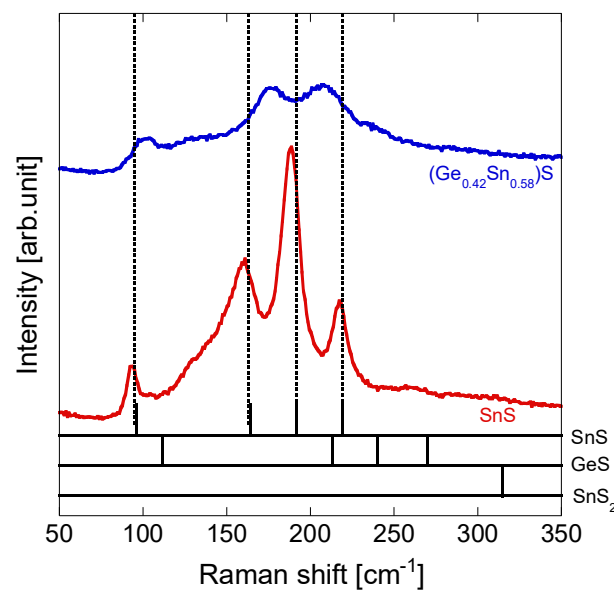


Figure 3. Raman spectra of the fabricated SnS [32] and $(\text{Ge}_{0.42}\text{Sn}_{0.58})\text{S}$ (red and blue lines, respectively) thin films. The reference Raman spectra of SnS [35], GeS [36], and SnS_2 [37] are shown by black lines at the bottom of the figure.

Figure 4a shows the SEM surface morphology of SnS. Block-like and plate-like crystal grains were observed on the SnS surface; these grains are commonly observed in SnS [39]. Figure 4b shows the surface morphology of $(\text{Ge}_{0.42}\text{Sn}_{0.58})\text{S}$. The observed grains are elongated platelets. The observed 1–5 μm grains, which are considerably larger than those of SnS, are thought to be due to the crystal growth of microcrystal grains by annealing. Sinsermsuksakul et al. reported that as the film thickness increased, the $\{010\}$ plane switched its crystallographic orientation from parallel to perpendicular to the substrate [17]. This suggests that the difference in the morphology of SnS and $(\text{Ge}_{0.42}\text{Sn}_{0.58})\text{S}$ may be partly due to the difference in film thickness. From the aforementioned XRD results, the $(\text{Ge}_{0.42}\text{Sn}_{0.58})\text{S}$ thin film was not preferentially oriented in one direction, but the orientation of each grain was considered to be different, as peaks that can be attributed to (111) and (040) are observed in the film. They have also pointed out that the plane perpendicular to the substrate is a desirable structure for solar cells because it significantly improves the mobility in the thickness direction compared to the plane parallel to the substrate [17]. The differences in contrast between the individual grains observed in Figure 4b may be due to differences in conductivity resulting from differences in orientation.

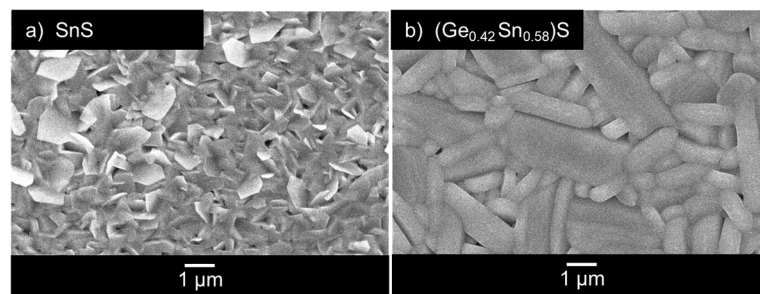


Figure 4. Surface morphology of (a) SEM images of surface morphology at different locations on the same sample as SnS in Ref. [32] and (b) $(\text{Ge}_{0.42}\text{Sn}_{0.58})\text{S}$ (annealed), observed using SEM. A white scale bar is shown at the bottom of the figure.

Figure 5a and Table 3 show the J - V curves and photovoltaic characteristics of SnS and $(\text{Ge}_{0.42}\text{Sn}_{0.58})\text{S}$ thin-film solar cells. The solar cells fabricated using SnS thin films showed an open circuit voltage (V_{oc}) of 0.053 V, short circuit current density (J_{sc}) of 9.00 mA/cm², fill factor (FF) of 0.32, and power conversion efficiency (PCE) of 0.15%. Contrarily, solar cells fabricated using the $(\text{Ge}_{0.42}\text{Sn}_{0.58})\text{S}$ thin film showed a V_{oc} of 0.29 V, J_{sc} of 6.92 mA/cm², FF of 0.34, and PCE of 0.67%. The $(\text{Ge}_{0.42}\text{Sn}_{0.58})\text{S}$ device showed a higher V_{oc} than the SnS device, with similar values of FF . The efficient formation of a p-n junction interface between the n-type CdS and p-type (Ge, Sn)S possibly improved the V_{oc} of the $(\text{Ge}_{0.42}\text{Sn}_{0.58})\text{S}$ device; the V_{oc} value of the device fabricated here is greater than those of previously reported solar cells based on $(\text{Ge}_{0.27}\text{Sn}_{0.73})\text{S}$ thin films [32]. The V_{oc} deficit $V_{ocdef} = V_{oc} - E_g/q$ (V), the difference between the band gap and the open circuit voltage estimated from the absorption edge of the EQE, which will be discussed below, was $V_{ocdef} = 1.217$ V for $x = 0$ ($E_g = 1.27$ eV). For $x = 0.42$ ($E_g = 1.42$ or 1.52 eV), $V_{ocdef} = 1.13$ or 1.23 V. This large V_{ocdef} indicates that significant recombination occurs in both samples. As the V_{ocdef} is almost the same magnitude for both samples, the change in V_{oc} can be attributed to the increase in band gap due to the introduction of Ge. This could be due to an increase in the band gap of the optical absorption layer due to an increase in the Ge concentration and the formation of large crystal grains due to the annealing process. Furthermore, the J_{sc} of the solar cell based on $(\text{Ge}_{0.42}\text{Sn}_{0.58})\text{S}$ thin films was slightly lower than that based on SnS thin films, possibly due to the presence of different phases, such as GeS_2 and Sn_2S_3 , which promoted recombination. Figure 5b shows the EQE of the fabricated SnS and $(\text{Ge}_{0.42}\text{Sn}_{0.58})\text{S}$ thin-film solar cells. The highest EQE was recorded at about 530 nm for both devices, possibly because only the carriers near the light absorption layer (SnS or $(\text{Ge}_{0.42}\text{Sn}_{0.58})\text{S}$)/CdS interface were extracted; carriers that were excited deep inside the light absorption layer (near the Mo back electrode) underwent recombination due to the short diffusion length of the carriers, and could not be extracted. The energy E versus $[E \ln(1-\text{EQE})]^2$ plots for the SnS and $(\text{Ge}_{0.42}\text{Sn}_{0.58})\text{S}$ thin-film solar cells are shown in Figure 5c and d, respectively. The band gap of SnS was estimated to be 1.28 eV by extrapolation, similar to the previously reported value [8,9,15,21–23]. The $(\text{Ge}_{0.42}\text{Sn}_{0.58})\text{S}$ spectrum shows a tail at the absorption edge, and its band gap was estimated to be in the range of 1.42–1.52 eV, indicating a non-uniform Ge concentration in (Ge, Sn)S, or absorption due to subgap defect levels.

Table 3. Photovoltaic characteristics of solar cells fabricated using the as-prepared SnS and $(\text{Ge}_{0.42}\text{Sn}_{0.58})\text{S}$ thin films.

| | Area [cm ²] | V_{oc} [V] | J_{sc} [mA/cm ²] | FF | PCE [%] |
|--|-------------------------|--------------|--------------------------------|------|-----------|
| SnS [32] | 0.1577 | 0.053 | 9.00 | 0.32 | 0.15 |
| $(\text{Ge}_{0.42}\text{Sn}_{0.58})\text{S}$ | 0.1514 | 0.29 | 6.92 | 0.34 | 0.67 |

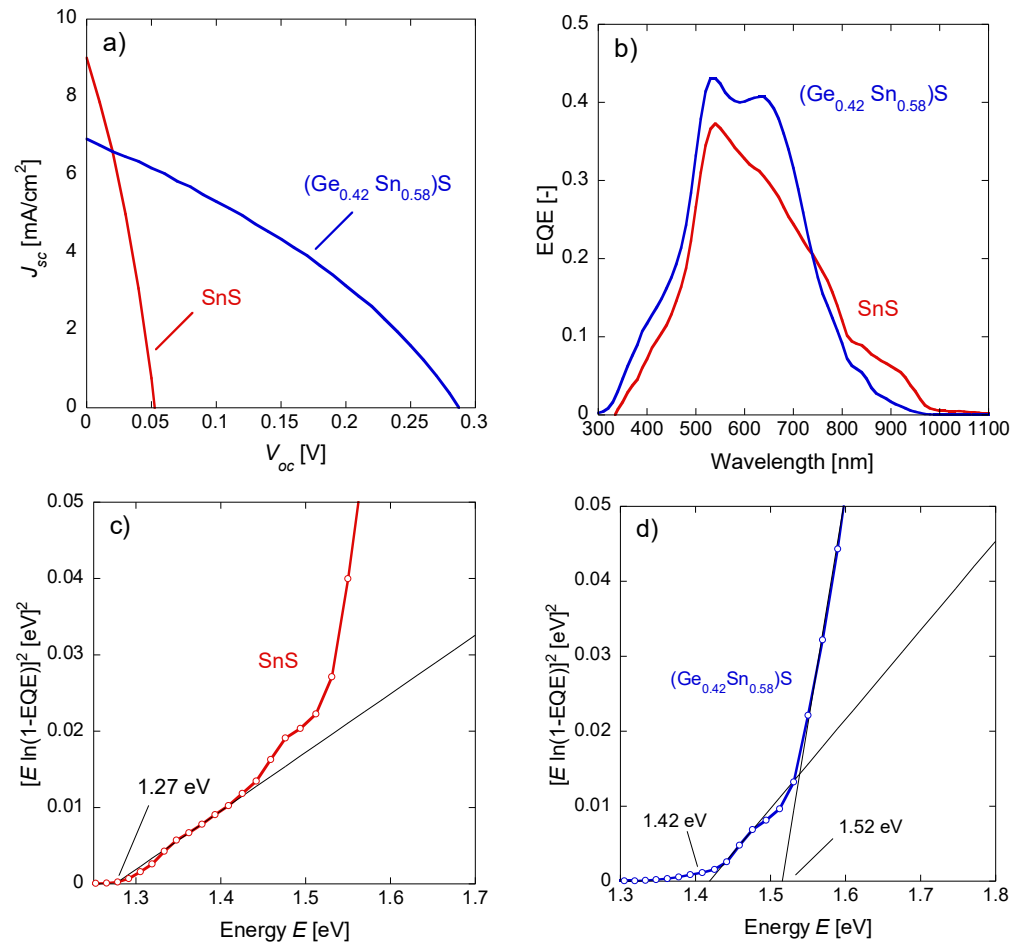


Figure 5. J-V curves and EQEs for the fabricated solar cells; the red and blue lines correspond to the SnS and (Ge_{0.42}Sn_{0.58})S thin-film solar cells, respectively. (a) J-V curves of solar cells fabricated with the SnS and (Ge_{0.42}Sn_{0.58})S thin films. (b) The EQEs of solar cells fabricated with the SnS and (Ge_{0.42}Sn_{0.58})S thin films. (c) Energy (E) versus $[E \ln(1-EQE)]^2$ plot and extrapolated line (black line) in the EQE plot of the SnS thin-film solar cell. (d) E versus $[E \ln(1-EQE)]^2$ plots and extrapolation lines for (Ge_{0.42}Sn_{0.58})S thin-film solar cells, similar to (c).

4. Conclusions

This study reports the synthesis of (Ge_{0.42}Sn_{0.58})S thin films using co-evaporation. XRD and Raman spectroscopy confirmed that a (Ge, Sn)S solid solution was formed in the (Ge_{0.42}Sn_{0.58})S thin film. The open circuit voltage (V_{oc}), short circuit current density (J_{sc}), FF , and PCE of solar cells fabricated using the (Ge_{0.42}Sn_{0.58})S thin film were 0.29 V, 6.92 mA/cm², 0.34, and 0.67%, respectively. Moreover, the bandgap of the (Ge_{0.42}Sn_{0.58})S thin-film solar cell was estimated to be 1.42–1.52 eV. In summary, in this study, we report the synthesis of a (Ge_{0.42}Sn_{0.58})S thin film with a Ge content of 0.42—confirmed to be a (Ge, Sn)S solid solution—and its application in solar cells. Among the (Ge, Sn)S solar cells reported thus far, it was clarified that solar cells can be realized even in a composition region with a relatively high Ge concentration. However, the photoelectric conversion characteristics are still inadequate, and improvements such as the suppression of thin-film crystal defects and the formation of appropriate heterojunction interfaces are required to improve the efficiency further. In addition, more detailed research on (Ge, Sn)S is required, such as the fabrication of (Ge, Sn)S thin films with even higher Ge concentrations and the realization of (Ge, Sn)S thin-film solar cells.

Author Contributions: Investigation and writing—original draft preparation, D.M.; writing—review, editing, and supervision, H.A. All authors have read and agreed to the published version of the manuscript.

Funding: This research was partially supported by JSPS KAKENHI (Grant Number JP 19H02663).

Data Availability Statement: Data are contained within the article.

Conflicts of Interest: The authors declare no conflicts of interest.

References

1. Green, M.A.; Dunlop, E.D.; Yoshita, M.; Kopidakis, N.; Bothe, K.; Siefert, G.; Hao, X. Solar cell efficiency tables (version 62). *Prog. Photovolt. Res. Appl.* **2023**, *31*, 651–663. [[CrossRef](#)]
2. Nair, P.K.; Garcia-Angelmo, A.R.; Nair, M.T.S. Cubic and orthorhombic SnS thin-film absorbers for tin sulfide solar cells. *Phys. Status Solidi A* **2016**, *213*, 170–177. [[CrossRef](#)]
3. Garcia-Angelmo, A.R.; Romano-Trujillo, R.; Campos-Alvarez, J.; Gomez-Daza, O.; Nair, M.T.S.; Nair, P.K. Thin film solar cell of SnS absorber with cubic crystalline structure. *Phys. Status Solidi A* **2015**, *212*, 2332–2340. [[CrossRef](#)]
4. Ahmet, I.Y.; Guc, M.; Sánchez, Y.; Neuschitzer, M.; Izquierdo-Roca, V.; Saucedo, E.; Johnson, A.L. Evaluation of AA-CVD deposited phase pure polymorphs of SnS for thin films solar cells. *RSC Adv.* **2019**, *9*, 14899. [[CrossRef](#)] [[PubMed](#)]
5. Norton, K.J.; Alam, F.; Lewis, D.J. A Review of the Synthesis, Properties, and Applications of Bulk and Two-Dimensional Tin (II) Sulfide (SnS). *Appl. Sci.* **2021**, *11*, 2062. [[CrossRef](#)]
6. Steinmann, V.; Jaramillo, R.; Hartman, K.; Chakraborty, R.; Brandt, R.E.; Poindexter, J.R.; Lee, Y.S.; Sun, L.; Polizzotti, A.; Park, H.H.; et al. 3.88% Efficient Tin Sulfide Solar Cells Using Congruent Thermal Evaporation. *Adv. Mater.* **2014**, *26*, 7488–7492. [[CrossRef](#)] [[PubMed](#)]
7. Kawano, Y.; Chantana, J.; Minemoto, T. Impact of growth temperature on the properties of SnS film prepared by thermal evaporation and its photovoltaic performance. *Curr. Appl. Phys.* **2015**, *15*, 897–901. [[CrossRef](#)]
8. Yago, A.; Kibishi, T.; Akaki, Y.; Nakamura, S.; Oomae, H.; Katagiri, H.; Araki, H. Influence of Sn/S composition ratio on SnS thin-film solar cells produced via co-evaporation method. *Jpn. J. Appl. Phys.* **2018**, *57*, 02CE08. [[CrossRef](#)]
9. Yago, A.; Sasagawa, S.; Akaki, Y.; Nakamura, S.; Oomae, H.; Katagiri, H.; Araki, H. Comparison of buffer layers on SnS thin-film solar cells prepared by co-evaporation. *Phys. Status Solidi C* **2017**, *14*, 1600194. [[CrossRef](#)]
10. Cifuentes, C.; Botero, M.; Romero, E.; Calderón, C.; Gordillo, G. Optical and structural studies on SnS films grown by co-evaporation. *Braz. J. Phys.* **2006**, *36*, 1046–1049. [[CrossRef](#)]
11. Arepalli, V.K.; Shin, Y.; Kim, J. Photovoltaic behavior of the room temperature grown RF-Sputtered SnS thin films. *Opt. Mater.* **2019**, *88*, 594–600. [[CrossRef](#)]
12. Zhao, L.; Di, Y.; Yan, C.; Liu, F.; Cheng, Z.; Jiang, L.; Hao, X.; Lai, Y.; Li, J. In situ growth of SnS absorbing layer by reactive sputtering for thin film solar cells. *RSC Adv.* **2016**, *6*, 4108–4115. [[CrossRef](#)]
13. Suzuki, I.; Kawanishi, S.; Bauers, S.R.; Zakutayev, A.; Lin, Z.; Tsukuda, S.; Shibata, H.; Kim, M.; Yanagi, H.; Omata, T. n-type electrical conduction in SnS thin films. *Phys. Rev. Mater.* **2021**, *5*, 125405. [[CrossRef](#)]
14. Kawanishi, S.; Suzuki, I.; Bauers, S.R.; Zakutayev, A.; Shibata, H.; Yanagi, H.; Omata, T. SnS Homo Junction Solar Cell with n-Type Single Crystal and p-Type Thin Film. *Sol. RRL* **2021**, *5*, 2000708. [[CrossRef](#)]
15. Sugiyama, M.; Reddy, K.T.R.; Revathi, R.; Shimamoto, Y.; Murata, Y. Band offset of SnS solar cell structure measured by X-ray photoelectron spectroscopy. *Thin Solid Films* **2011**, *519*, 7429–7431. [[CrossRef](#)]
16. Minemura, T.; Miyauchi, K.; Noguchi, K.; Ohtsuka, K.; Nakanishi, H.; Sugiyama, M. Preparation of SnS films by low-temperature sulfurization. *Phys. Status Solidi C* **2009**, *6*, 1221–1224. [[CrossRef](#)]
17. Sinersuksakul, P.; Heo, J.; Noh, W.; Hock, A.S.; Gordon, R.G. Atomic Layer Deposition of Tin Monosulfide Thin Films. *Adv. Energy Mater.* **2011**, *1*, 1116–1125. [[CrossRef](#)]
18. Sinersuksakul, P.; Sun, L.; Lee, S.W.; Park, H.H.; Kim, S.B.; Yang, C.; Gordon, R.G. Overcoming Efficiency Limitations of SnS-Based Solar Cells. *Adv. Energy Mater.* **2014**, *4*, 1400496. [[CrossRef](#)]
19. Choi, Y.; Park, H.; Lee, N.; Kim, B.; Lee, J.; Lee, G.; Jeon, H. Deposition of the tin sulfide thin films using ALD and a vacuum annealing process for tuning the phase transition. *J. Alloys Compd.* **2022**, *896*, 162806. [[CrossRef](#)]
20. Higareda-Sánchez, A.; Mis-Fernández, R.; Rimmaudo, I.; Camacho-Espinosa, E.; Peña, J.L. Evaluation of pH and deposition mechanisms effect on tin sulfide thin films deposited by chemical bath deposition. *Superlattices Microstruct.* **2021**, *151*, 106831. [[CrossRef](#)]
21. Araki, H.; Abe, M.; Yago, A.; Katagiri, H.; Akaki, Y. Preparation of SnS Thin Films Using Close Space Sublimation. *J. Nanoelectron. Optoelectron.* **2019**, *12*, 920–924. [[CrossRef](#)]
22. Lin, D.-Y.; Hsu, H.-P.; Liu, K.-H.; Wu, P.-H.; Shih, Y.-T.; Wu, Y.-F.; Wang, Y.-P.; Lin, C.-F. Enhanced Optical Response of SnS/SnS₂ Layered Heterostructure. *Sensors* **2023**, *23*, 4976. [[CrossRef](#)]
23. Noguchi, H.; Setiyadi, A.; Tanamura, H.; Nagatomo, T.; Omoto, O. Characterization of vacuum-evaporated tin sulfide film for solar cell materials. *Sol. Energy Mater. Sol. Cells* **1994**, *35*, 325–331. [[CrossRef](#)]
24. Reddy, K.T.R.; Reddy, N.K.; Miles, R.W. Photovoltaic properties of SnS based solar cells. *Sol. Energy Mater. Sol. Cells* **2006**, *90*, 3041–3046. [[CrossRef](#)]
25. Ikuno, T.; Suzuki, R.; Kitazumi, K.; Takahashi, N.; Kato, N.; Higuchi, K. SnS thin film solar cells with Zn_{1-x}Mg_xO buffer layers. *Appl. Phys. Lett.* **2013**, *102*, 193901. [[CrossRef](#)]

26. Cho, J.Y.; Kim, S.Y.; Nandi, R.; Jang, J.; Yun, H.-S.; Enkhbayar, E.; Kim, J.H.; Lee, D.-K.; Chung, C.-H.; Kim, J.H.; et al. Achieving over 4% efficiency for SnS/CdS thin-film solar cells by improving the heterojunction interface quality. *J. Mater. Chem. A* **2020**, *8*, 20658–20665. [[CrossRef](#)]
27. Yun, H.-S.; Park, B.; Choi, Y.C.; Im, J.; Shin, T.J.; Seok, S. Efficient Nanostructured TiO₂/SnS Heterojunction. *Sol. Cells Adv. Energy Mater.* **2019**, *9*, 1901343. [[CrossRef](#)]
28. Andrade-Arvizua, J.A.; García-Sánchez, M.F.; Courel-Piedrahíta, M.; Pulgarín-Agudelo, F.; Santiago-Jaimes, E.; Valencia-Resendiz, E.; Arce-Plazac, A.; Vigil-Galána, O. Suited growth parameters inducing type of conductivity conversions on chemical spray pyrolysis synthesized SnS thin films. *J. Anal. Appl. Pyrolysis* **2016**, *121*, 347–359. [[CrossRef](#)]
29. Yanagi, H.; Iguchi, Y.; Sugiyama, T.; Kamiya, T.; Hosono, H. N-type conduction in SnS by anion substitution with Cl. *Appl. Phys. Express* **2016**, *9*, 051201. [[CrossRef](#)]
30. Kawamura, F.; Song, Y.; Murata, H.; Tampo, H.; Nagai, T.; Koida, T.; Imura, M.; Yamada, N. Tunability of the bandgap of SnS by variation of the cell volume by alloying with A.E. elements. *Sci. Rep.* **2022**, *12*, 7434. [[CrossRef](#)]
31. Im, H.Y.; Myung, Y.; Park, K.; Jung, C.S.; Lim, Y.R.; Jang, D.M.; Park, J. Ternary alloy nanocrystals of tin and germanium chalcogenides. *RSC Adv.* **2014**, *4*, 15695–15701. [[CrossRef](#)]
32. Motai, D.; Tasaki, T.; Araki, H. Fabrication of solar cell using Ge-Sn-S thin film prepared by co-evaporation. *Jpn. J. Appl. Phys.* **2023**, *62*, SK1037. [[CrossRef](#)]
33. Motai, D.; Ohashi, R.; Araki, H. Effect of annealing temperature on p–n junction formation in Cu₂SnS₃ thin-film solar cells fabricated via the co-evaporation of elemental precursors. *Jpn. J. Appl. Phys.* **2022**, *61*, SB1043. [[CrossRef](#)]
34. Malone, B.D.; Gali, A.; Kaxiras, E. First principles study of point defects in SnS. *Phys. Chem. Chem. Phys.* **2014**, *16*, 26176–26183. [[CrossRef](#)]
35. Li, M.; Wu, Y.; Li, T.; Chen, Y.; Ding, H.; Lin, Y.; Pan, N.; Wang, X. Revealing anisotropy and thickness dependence of Raman spectra for SnS flakes. *RSC Adv.* **2017**, *7*, 48759–48765. [[CrossRef](#)]
36. Tan, D.; Lim, H.E.; Wang, F.; Mohamed, N.B.; Mouri, S.; Zhang, W.; Miyauchi, Y.; Ohfuchi, M.; Matsuda, K. Anisotropic optical and electronic properties of two-dimensional layered germanium sulfide. *Nano Res.* **2017**, *10*, 546–555. [[CrossRef](#)]
37. Stetsenko, M.O.; Voznyi, A.A.; Kosyak, V.V.; Rudenko, S.P.; Maksimenko, L.S.; Serdega, B.K.; Opanasuk, A.S. Plasmonic Effects in Tin Disulfide Nanostructured Thin Films Obtained by the Close-Spaced Vacuum Sublimation. *Plasmonics* **2016**, *12*, 1213–1220. [[CrossRef](#)]
38. Araki, H.; Yamano, M.; Nishida, G.; Takeuchi, A.; Aihara, N.; Tanaka, K. Synthesis and characterization of Cu₂Sn_{1-x}Ge_xS₃. *Phys. Stat. Sol.* **2014**, *14*, 1600199. [[CrossRef](#)]
39. Banai, R.E.; Horn, M.W.; Browson, J.R.S. A review of tin (II) monosulfide and its potential as a photovoltaic absorber. *Sol. Energy Mater. Sol. Cells* **2016**, *150*, 112–129. [[CrossRef](#)]

Disclaimer/Publisher’s Note: The statements, opinions and data contained in all publications are solely those of the individual author(s) and contributor(s) and not of MDPI and/or the editor(s). MDPI and/or the editor(s) disclaim responsibility for any injury to people or property resulting from any ideas, methods, instructions or products referred to in the content.